Holocene variability in Upper Circumpolar Deep Water on the West Antarctic Peninsula.

Victoria L. Peck[1*], Claire S. Allen[1], Sev Kender[2, 3], Erin L. McClymont[4] and Dominic Hodgson[1,4].

1. British Antarctic Survey, High Cross, Madingley Rd, Cambridge CB3 0ET, UK.
2. University of Nottingham, School of Geography, Nottingham, NG7 2RD, UK.
3. British Geological Survey, Keyworth, Nottingham, NG12 5GG, UK.
4. Durham University, Department of Geography, South Road, Durham, DH1 3LE, UK.

*corresponding author - vlp@bas.ac.uk

Recent intensification of wind-driven upwelling of warm upper circumpolar deep water (UCDW) has been linked to recent accelerated melting of West Antarctic ice shelves and glaciers. To better assess the long term relationship between UCDW upwelling and the West Antarctic Ice Sheet, we present a multi-proxy reconstruction of surface and bottom water conditions in Marguerite Bay, West Antarctic Peninsula (WAP), through the Holocene. A combination of sedimentological, diatom and foraminiferal records are, for the first time, presented together and demonstrate the decline in UCDW influence within Marguerite Bay through the early to mid Holocene and the onset of cyclic forcing in the late Holocene. We show that persistent incursions of UCDW between 9707 to 6903 yr BP (modelled ages) restricted sea ice formation, enhanced primary productivity and promoted basal melting of ice shelves. From 6903 kyr BP the influence of UCDW in Marguerite Bay waned, coincident with the equatorward migration of the Southern Hemisphere Westerly Winds (SWW). Weakening UCDW influence continued through the mid Holocene and by 4153 yr BP lengthy sea ice seasons within Marguerite Bay were only episodically interrupted by incursions of UCDW. The late Holocene interval, from 4153 kyr BP, appears to have been sensitive to ENSO forcing as opposed to the SWW-forcing that dominated the early to mid Holocene. Current measurements of the oceanography of the WAP continental shelf suggest that the system has returned to the early Holocene-like oceanographic configuration reported here, which in both cases has been associated with rapid deglaciation.

1. INTRODUCTION

Relatively warm (>1°C), nutrient rich and CO_2 saturated upper circumpolar deep water (UCDW) is transported around the Antarctic continent in the Antarctic Circumpolar Current, which is in turn driven by the Southern Hemisphere Westerly Winds (SWW). Where the Antarctic Circumpolar Current flows close to the Antarctic continental shelf edge, along the West Antarctic Peninsula (WAP), Bellingshausen and Amundsen Seas, upwelled-UCDW frequently spills onto the shelf via bathymetric troughs, circulating relatively warm water under ice shelves and contributing to their retreat (Jacobs et al., 2011; Jenkins and Jacobs, 2008; Wåhlin et al., 2010; Walker et al., 2007). More frequent and/or stronger incursions of UCDW are believed to contribute to recent, rapid warming (Vaughan et al., 2003), accelerated ice sheet thinning (Pritchard et al., 2012), reduced sea ice extent and notable changes in phytoplankton communities (Montes-Hugo et al., 2009) along the WAP in recent decades (Ducklow et al., 2012). The rapid deglacial retreat of the Marguerite Bay ice stream from ~9.6 kyr BP, is widely considered to have been driven by enhanced incursions of warm UCDW encroaching onto the WAP continental shelf (Bentley et al., 2011; Kilfeather et al., 2011). While predicted intensification of the SWW in coming years (Swart and Fyfe, 2012) may continue to promote UCDW upwelling and further threaten WAP ice shelf stability, a consensus on how UCDW along the WAP responded to changing SWW in the past has yet to be achieved (Ishman and Sperling, 2002; Shevenell and Kennett, 2002; also see discussion in Bentley et al., 2009). The aim of this paper was to assess the sensitivity of UCDW upwelling along the WAP to past changes in SWW by analysing the exceptionally well preserved planktonic and benthic foraminifera, diatoms and pigments in marine sediment core TPC522, Marguerite Bay (Fig. 1). These biogenic components provide proxies for reconstructing past surface and bottom water conditions and documenting the changing influence of UCDW on

the inner WAP continental shelf. We compare these reconstructions with other Southern Hemisphere records to infer the sensitivity of UCDW-upwelling to SWW intensity and position and the impact of UCDW-upwelling on deglaciation.

1.1. Regional setting

Piston core TPC522, collected on British Antarctic Survey cruise JR179 in 2008 recovered 11.7 m of sediment from inner Marguerite Bay (67° 51'.33 S 68° 12'.28 W; Fig. 1). The site of TPC522, in 910 m of water, is downstream of Marguerite Trough which funnels UCDW directly from the continental shelf edge, where the Antarctic Circumpolar Current spills into bathymetric lows (Klinck et al., 2004; Martinson et al., 2008; Moffat et al., 2009). These incursions of UCDW are modified and cooled through mixing with overlying relatively cold and fresh Antarctic Surface Water (AASW) such that modified UCDW floods the continental shelf to the base of the pycnocline (Martinson et al., 2008; Fig.2A). The presence of UDCW beneath the pycnocline on the WAP is identified by temperature and salinity maxima as well as oxygen minima (Klinck et al., 2004). Being enriched in nutrients and remineralised organic matter, UCDW is also depleted in ^{13}C and has diagnostic benthic $\delta^{13}C$ values <0.4 ‰ (Mackenesen, 2012). Deep mixing of the AASW occurs during the winter months when UCDW-derived heat and nutrients may be incorporated into surface waters (Smith et al., 1999; Prezelin et al., 2000). Subsequent stratification during the summer months as temperatures rise and ice melts is associated with intense primary productivity (e.g. Prezelin et al., 2000) and the occurrence of a remnant Winter Water temperature minimum at 50-150 m water depth (Meredith et al., 2013; see Fig. 2A). Mixing of UCDW within surface waters is therefore recognised by enhanced primary productivity (Prezelin et al., 2000) and reduced sea ice extent (Martinson et al., 2008).

2. METHODS

The chronology of TPC522 is based on twelve acid insoluble organic matter (AIOM), and one monospecific benthic foraminifera (*Globocassidulina biora*) radiocarbon dates. Dates were calibrated using CALIB 6.0 using the MARINE09 calibration curve (Stuiver & Reimer, 1993). ΔR was set at 1353 years based on a local mean surface sample radiocarbon age of 1753 ^{14}C yr BP from box cores BC523 (at the site of TPC522) and BC521 (9.2 km distant) minus the global ocean reservoir correction of 400 years. Dates are reported as conventional radiocarbon years BP (^{14}C yr BP) ±1σ and in calibrated years BP (cal yr BP relative to AD 1950; Table 1). Classical radiocarbon age-depth modelling was undertaken using CLAM v, 2.1 software in R (Blaauw, 2010) using a smooth spline curve fit, running 1000 iterations at 1 cm intervals (Fig. 3A). To independently date the surface sediments, excess ^{210}Pb activity was measured on thirteen downcore samples in the top 23 cm of BC523 using a J- shaped ultra low background germanium well detection system at Durham University. Data analysis and dating model calculations were undertaken following the standard procedures defined in Appleby (2001).

For foraminifera and ice rafted debris (IRD) analysis, samples of ~2 cm^3 were collected at up to 5 cm intervals, then weighed and sieved through a 63 μm mesh using de-ionised water. The residues were dried at 45 °C. Separate samples were collected every 10 cm for wet and dry weight and bulk density measurements without risking the integrity of the foraminiferal geochemistry. Dried samples from 10 to 20 cm intervals were sieved through a 125 μm sieve. Samples with abundant foraminifera were split with a microsplitter prior to sieving. At least 100 specimens of benthic foraminifera were counted per sample wherever possible. Between 5 and 20 specimens of *N. pachyderma* sin. and *B. aculeata* were picked from each sample wherever possible for stable isotope analysis. Stable isotope analyses were

carried out using a VG PRISM mass spectrometer at the Godwin Laboratory, Cambridge and were measured relative to the Vienna Peedee Belemnite (VPDB) with reproducibility <0.08 ‰ for $\delta^{18}O$ and <0.06 ‰ for $\delta^{13}C$. The concentration of glacial debris was determined from counts of terrigenous grains from the >150 μm size fraction.

For diatom counts the quantitative slide preparation method of Scherer (1994) was used and counting was carried out at ×1000 magnification on an Olympus BX42 microscope. Taxonomy followed Tomas (1997), supplemented by Fenner et al. (1976) and Johansen and Fryxell (1985). To extract the most detailed environmental information from the diatom record, species morphotypes *Thalassiosira antarctica* T1 and T2 (cold and warm varieties, respectively; Buffen et al., 2007) and *Eucampia antarctica* var. *antartica* and var. *recta* (symmetrical and asymmetrical forms respectively) were counted separately (Leventer et al., 2002; Allen, 2014). *Chaetoceros* resting spores (CRS) comprise at least 82 % of the diatom assemblage throughout TPC522. In order to extract the ecological information from the minor species assemblages, CRS-free counts are presented based on minimum counts of 400 valves (excluding CRS) per slide. For statistical analyses, only diatom species that accounted for >2 % of the CRS-free assemblage within at least one sample were included. Correspondence analysis (CA) was performed on both the diatom and benthic foraminferal assemblage counts using the software of Hammer et al. (2005).

For pigment analysis, bulk sediment samples were freeze-dried and homogenised. Approximately 2 g of sample was extracted with an organic solvent mixture of dichloromethane/methanol (DCM/MeOH, 3:1, v/v), using a microwave assisted extraction (Kornilova and Rosell-Mele, 2003). The temperature of the microwave was increased up to 70 ºC over 2 minutes, held at 70 ºC for 5 min and then allowed to cool. Extracts were transferred to test tubes, centrifuged, and the supernatant dried by rotary evaporation. Samples were redissolved in a known volume of acetone and transferred to a 2 ml quartz

cuvette for analysis in a WPA spectrophotometer. Absorbance was recorded by measurements in triplicate at the wavelengths 410 nm and 665 nm, which correspond to the diagenetic transformation products of chlorophyll, the chlorins (Harris et al., 1996).

3. RESULTS

3.1 AGE-DEPTH MODEL

The excess ^{210}Pb activity profile confirmed that the upper sediments were deposited within recent decades (Fig. 3B). The surface sediment radiocarbon ages are therefore considered a reliable indication of the modern ^{14}C reservoir age at this site, although older reservoir ages have been reported in this region (Kilfeather et al., 2011; Graham & Smith, 2012). Total organic carbon values were relatively consistent downcore (0.9-1.7 %) and mean $\delta^{13}C_{AIOM}$ was -21.6 ‰ with a standard deviation of 0.8 ‰ indicating that AIOM used for radiocarbon dating was consistently of marine origin with no evidence of variable terrestrial input. The AIOM age at 955 cm and benthic foraminifera sample at 1000 cm have overlapping calibrated age ranges suggesting that the radiocarbon reservoir in the AIOM may be slightly larger towards the base of the core (see Rosenheim et al., 2013). We considered the conventional radiocarbon age 6420±40 at 350 cm an unrealistic age-reversal and omitted it from our age-depth model, although the $\delta^{13}C_{AIOM}$ does not suggest it was of a different origin. The radiocarbon date at the top of PC522 (0-2 cm) gives a calibrated and corrected age of 292-461 years suggesting the piston corer may have slightly over-penetrated the surface.

3.2 STATISTICAL ANALYSIS OF ASSEMBLAGES

The first three axes of the CA accounted for 57% and 66% of the variance in the diatom and foraminifera assemblages respectively (Fig. 4). Significant assemblage shifts (> 1

s.d.) were used to identify three stratigraphic intervals that approximately corresponding to the early, mid and late Holocene. Boundaries between these stratigraphic intervals are at near identical depths in the diatom and benthic foraminiferal records suggesting a close coupling of surface and benthic conditions within inner Marguerite Bay. The early Holocene interval begins at 9707 yr BP (best fit from the CLAM age-depth model with 95 % confidence levels for these dates being 9618-9835 yr BP). Based on diatom assemblage change the early Holocene interval extends to 6903 yr BP (95% confidence levels for this date being 6820-6984 yr BP) and the benthic foraminifera assemblage change at 6992 yr BP (95% confidence levels being 6907-7070 yr BP). The mid Holocene interval ends at 4213 yr BP based on the diatom assemblage (with 95% confidence levels for this date being 4066-4341 yr BP) and 4153 yr BP based on the benthic foraminifera assemblage (with 95% confidence levels being 4008-4274 yr BP). From hereon in the single best fit date from the CLAM age-depth model will be given.

3.3 DIATOM ASSEMBLAGES

Interpretations of the diatom and foraminifera assemblages were based on the auto-ecological data presented in supplementary Table 1. The early Holocene diatom assemblage (9707 to 6992 yr BP), characterised by *Thalassiosira tumida, Eucampia antarctica* (Fig. 5F), *Thalassiosira gracilis* and *Proboscia truncata*, is indicates reflect relatively warm surface waters with a long growth season, minor sea ice influence and rich in iron; most likely associated with seasonal glacial melt and late summer/autumn productivity (Stickley et al., 2006; Allen et al., 2010).The high ratio of asymmetrical:symmetrical morphotypes of *E. antarctica* (Fig. 5G) is consistent with relatively high sea surface temperatures (SST; Leventer et al., 2002). *F. kerguelensis* is an open ocean species, used as a tracer for Antarctic Circumpolar Current waters entrained onto the continental shelf (Bathmann et al., 1991;

Allen et al., 2010) or carried beyond the Southern Ocean (Stickley et al., 2001; Romero and Hensen, 2002). Therefore the high relative abundance of open-water *F. kerguelensis* (Fig. 5D), within TPC522 suggests that the site was bathed by UCDW in the early Holocene. In the mid Holocene (6903 to 4213 yr BP) the diatom assemblage shows a decline *E. antarctica* and increases in *Thalassiosira antarctica* (cold morphotype; Fig. 5E) and *P. truncata*. This shift in assemblage is interpreted as an increasing marginal sea ice influence, including the presence of ice during the summer months (Pike et al., 2009), and a shortening of the growth season. The persistent occurrence of *F. kerguelensis* during the mid Holocene interval suggests that UCDW continued to bathe our site. The ratio of asymmetrical:symmetrical morphotypes of *E. antarctica* peaks between 6903 and 5882 yr BP suggesting the warmest SSTs of our record, before falling through the mid to late Holocene. The late Holocene diatom assemblage (from 4213 yr BP) is marked by a very low abundance of the high nutrient, warm, open-water assemblages of the early Holocene (i.e. *T. tumida, E. antarctica,* and *F. kerguelensis*) and instead is characterised by sea ice proximal species (*Fragilariopsis curta, Fragilariopsis cylindrus* and Parmales (Zielinski, 1997). This transition from the mid to late Holocene assemblages is also marked by a prominent peak in the flux of diatoms accumulation at the sea floor suggesting a brief interval of exceptionally high primary productivity. Relatively high fluxes of diatoms continue to 2584 yr BP. The late Holocene diatom assemblage reflects a significant sea ice influence and further shortening of the growth season and declining productivity (diatom flux).

3.4 BENTHIC FORAMINIFERAL ASSEMBLAGES

Extensive dissolution of calcareous foraminfera can occur in sediments collected from the WAP (Osterman et al., 2001). However, since the concentration of benthic foraminifera in TPC522 exceeds that within ODP Site 1098 by orders of magnitude throughout the Holocene

(Supplemetary Fig. 1) we consider dissolution to be less of an issue at TPC522 site compared to Palmer Deep. SEM images from numerous depths are also provided (supplementary plates 1 and 2).

The early Holocene benthic foraminiferal assemblage (9707 to 6992 yr BP) is largely comprised of *Fursenkoina fusiformis* and *Nonionella* spp. (Fig. 5K, L). These species are commonly associated with sites subject to intense pulses of phytodetritus (Gooday, 2003; Gooday et al. 2012) and organic-rich, low-oxygen settings (Sen Gupta and Machain-Castillo, 1993; Ishman and Domack, 1994). Along the WAP these species occur in surface sediment samples of the Bransfield Strait (Ishman and Domack, 1994) and the Weddell Sea shelf (Mackensen et al., 1990), where there is high productivity and high particulate organic carbon export (Mackensen et al., 1990). Although it has been suggested that the modern *Fursenkoina/Nonionella* assemblage in the Bransfield Strait is primarily indicative or Weddell Sea Water (Ishman and Domack, 1994), the interpretations of Ishman and Sperling (2002) and Kilfeather et al. (2011), that assemblages with high proportions of these species are most likely tracking high productivity and organic carbon flux to the sea floor, is more consistent with our other proxy data (see later discussion). In addition, Weddell Sea Water is not known to reach this far south along the WAP (Martinson et al., 2008). The mid Holocene foraminiferal assemblage (6992 to 4153 yr BP) is dominated by *Bulimina aculeata* (Fig. 5N). *B. aculeata*, is associated organic-rich sediments (Mackensen et al. 1993) and has been used as an UCDW tracer (Ishman and Domack, 1994) at Palmer Deep (Ishman & Sperling 2002) and Lützow-Holm Bay (Igarashi et al. 2001). The late Holocene foraminiferal assemblage (from 4153 kyr BP) oscillates between the *B. aculeata* assemblage of the mid Holocene and predominantly agglutinated species (Fig. 5M).The agglutinated assemblage, dominated by *Miliamina arenacea* and including *Trochammina* spp. and *Reophax* spp., is typical of the agglutinated assemblages which characterise cold saline shelf water around Antarctica

(Ishman & Domack, 1994; Ishman & Sperling, 2002; Anderson, 1975; Milam & Anderson 1981; Majewski & Anderson, 2009). The oscillation between these two foraminiferal assemblages suggests switching between two oceanographic modes; most likely the presence of UCDW associated with the *B. aculeata* assemblage, and the presence of cold, saline shelf water associated with the *M. arenacea* assemblage (Ishman & Sperling, 2002). These assemblage oscillations are evident on a decadal to centennial timescale through the high sedimentation up to 2679 yr BP and inferred to have persisted throughout the remainder of the record but compromised by low sedimentation rates (<1 mm yr^{-1} from 2679 yr BP) which may have caused the signal to become homogenised.

3.5 STABLE ISOTOPES

Since foraminifera do not necessarily precipitate their carbonate in equilibrium with seawater $\delta^{18}O_{seawater}$ we compared our records with predicted $\delta^{18}O_{CaCO3}$ values to establish whether it was necessary to apply a vital effect correction to either of the measured species. Predicted $\delta^{18}O_{CaCO3}$ for the entire water column was calculated from modern temperature and salinity data (JR179 cruise CTD025 collected 2nd April 2008, see Fig. 1 for locality and Fig. 2A for water column profile) following Shackleton (1974). Seawater $\delta^{18}O$ was estimated (Fig. 2B) from salinity using a relationship derived from local, contemporaneous salinity and isotope measurements, specifically $\delta^{18}O_{seawater} = 0.6486*S-22.536$ (see data in Meredith et al., 2010). During the austral summer, at peak chlorophyll concentrations, *N. pachyderma* sin. is commonly found to calcify at pycnocline depths (Mortyn & Charles, 2003; Hendry et al., 2009). The predicted equilibrium $\delta^{18}O_{CaCO3}$ values at these calcification depths are consistent with the range of $\delta^{18}O_{N.\ pachyderma\ sin.}$ values from surface sediments reported here, when a vital effect correction of 0.63 ‰ is applied (Bausch et al., 1997). This vital effect correction is

similar to that applied to *N. pachyderma* sin. specimens collected in sediment traps during 2005-2006 at the nearby Rothera Oceanographic and Biological Time-Series site (Hendry et al., 2009). The $\delta^{18}O$ values we measured from surface sediment samples are within the range of those reported in Hendry et al. (2009; see Fig. 5P), although at the heavier end of the range suggesting that *N. pachyderma* sin. is currently calcifying in warmer and/or fresher waters today than the recent decades when our sediment surface specimens would represent. Surface sediment $\delta^{18}O_{B.\ aculeata}$ values with no vital effect correction compare well with predicted equilibrium $\delta^{18}O_{CaCO3}$ values at the sea floor consistent with *Bulimia* spp. precipitating $\delta^{18}O$ in equilibrium with seawater (cf. Barras et al., 2010; Grossman, 1987).

The stable and consistently offset benthic and planktonic $\delta^{18}O$ values throughout the early Holocene interval are consistent with a persistent density structure between the pycnocline and sea floor, at least during the growth season of *N. pachyderma* sin., which is comparable to today (Fig. 2B). This density structure would suggest that, similarly to today (see Martinson et al., 2008), modified-UCDW flooded the water column to the base of the pycnocline across the shelf and into Marguerite Bay. The slight decrease in benthic and planktonic $\delta^{18}O$ through the early Holocene would be consistent with warming and/or increased glacial melt water input. The low $\delta^{13}C_{N.\ pachyderma\ sin.}$ values (Fig. 5O) through the early Holocene could result from high primary productivity and remineralisation of ^{12}C-enriched organic matter below the mixed layer, diffusive mixing of ^{13}C-depleted UCDW through the pycnocline (Mackensen, 2012) or *N. pachyderma* sin. inhabiting sea ice (Hendry et al,.2009). Given the low abundance of sea ice diatoms, the high fluxes of *N. pachyderma* sin. indicative of open water conditions and the relative warm SSTs suggested by the ratio of asymm:symm *E. antarctica* we suggest that it is highly unlikely that the decreased $\delta^{13}C_{N.\ pachyderma\ sin.}$ during the early Holocene resulted from these species inhabiting sea ice. Our

multi-proxy dataset therefore favours an interpretation where the similar and low benthic and planktonic $\delta^{13}C$ values observed in the early Holocene result from diffusive mixing of nutrient-rich, ^{13}C-depleted UCDW through the pycnocline and remineralisation of relatively high volumes of organic matter exported from surface waters. We acknowledge that in some cases $\delta^{13}C$ from infaunal benthic foraminifera may not be entirely representative of benthic water values, however we propose that the persistently low benthic $\delta^{13}C$ values recorded at TPC522 throughout the early and mid Holocene are consistent with modified-UCDW maintaining a constant presence at depth within inner Marguerite Bay.

A positive shift in planktonic $\delta^{13}C$ of 2 ‰ from at least 6992 yr BP, generating an offset between benthic and planktonic $\delta^{13}C$ records of ~0.8 ‰, indicates ^{13}C-stratification of the water column occurred at the onset of the mid Holocene interval. A 0.3 ‰ increase in the benthic $\delta^{13}C$ record also occurred at the onset of the mid Holocene, although as stated above, the persistently low $\delta^{13}C_{\textit{B. aculeata}}$ indicate that our site was continually bathed by modified-UCDW throughout the mid Holocene. We therefore consider the ^{13}C-stratification of the water column to be consistent with reduced mixing of modified-UCDW through the pycnocline during the winter months and significantly reduced export rates limiting remineralisation of ^{12}C-enriched organic matter beneath the mixed layer and to a lesser extent at the sea floor (contributing to the small amplitude change in the benthic $\delta^{13}C$ relative to the planktonic $\delta^{13}C$). This proposed reduction in UCDW influence in the sub-surface waters is not associated with a notable change in the planktonic $\delta^{18}O$ record, which maintains a persistent offset from the benthic $\delta^{18}O$ record until 4315 yr BP. The persistent off set between the benthic and planktonic $\delta^{18}O$ records suggests that seasonal stratification and the preservation of a Winter Water layer, as today, was a feature common to both the early and mid Holocene intervals.

Increased variability in both the planktonic and benthic stable isotope records from 4315 yr BP suggests significant shifts in sub-surface and benthic watermass properties at this site during the late Holocene. Convergence of planktonic and benthic $\delta^{18}O$ and positive benthic $\delta^{18}O$ excursions of up to 0.7 ‰, which may account for episodic cooling of benthic waters of up to 2 °C, suggest overturning of the water column and the displacement of modified-UCDW by a cold and/or more saline water mass. It should be noted that since the *B. aculeata*-assemblage is episodically displaced during the late Holocene by the agglutinate dominated-assemblage, considered to be associated with cold, saline waters which are inhospitable to calcareous species, our benthic stable isotope record may not fully represent intervals of UCDW-displacement. However, the episodic overturn in the benthic foraminifera assemblage to one dominated by agglutinated species further supports the scenario for UCDW being displaced by cold, saline shelf waters.

4. DISCUSSION - MULTI-PROXY INTERPRETATION AND REGIONAL CONTEXT

4. 1 Early Holocene

Prior to 9707 yr BP, the retreat of the Marguerite Bay ice stream (Bentley et al., 2011; Kilfeather et al., 2011) is evident in our record from the high accumulation of glacial debris (Fig. 5A, 6A). Abundant Antarctic Circumpolar Current-derived *F. kerguelensis* and low benthic $\delta^{13}C$ values are consistent with the continuous advection of UCDW through the Marguerite Trough and over the core site through this early Holocene interval (Fig. 6B). Limited sea ice and extensive glacial melt, promoted by enhanced mixing of warm, modified-UCDW through the pycnocline is evidenced by mild, iron-rich and productive surface waters inferred from the high ratios of asymmetrical:symmetrical morphotypes of *E. antarctica*

(Leventer et al., 2002), high relative abundance of *E. antarctica* (Allen et al., 2010) and high Chl*a* concentrations (Fig. 5C) and planktonic foraminifera fluxes (Fig. 5H) respectively. These highly productive conditions are associated with depleted $\delta^{13}C$ values for *N. pachyderma* sin. which likely result from both diffusive mixing of ^{13}C-depleted UCDW through the pycnocline and remineralisation of enhanced fluxes of organic matter exported from the mixed layer. At the sea floor, relatively high accumulations (Fig. 5I) of a low diversity (Fig. 5J), small, thin-walled, infaunal benthic foraminifera (*F. fusiformis* and *Nonionella* spp.) are consistent with intense pulses of phytodetritus (Gooday, 2003; Gooday et al. 2012; Ishman and Sperling 2002). *B. aculeata*, commonly cited as an UCDW-indicator species (Ishman and Domack, 1994; Ishman and Sperling 2002), dominates the benthic fauna from 6992 yr BP. The low abundance of this species in the early Holocene, when all other proxies point to the prevalence of modified-UCDW throughout the water column above the site, may be due to out-competition by more opportunistic species or because oxygen levels were too low. While *B. aculeata*, is typically associated with organic-rich sediments (Gooday, 2003; Mackensen et al., 1993), and warm, moderately oxygenated bottom waters (Mackensen et al., 1990; Harloff and Mackensen, 1997), the small, thin-walled species *F. fusiformis* and *Nonionella* spp., which dominate the early Holocene interval, are able to tolerate exceptionally high fluxes of phytodetritus and oxygen depleted bottom waters (Gooday and Hughes, 2002; Gooday et al., 2012; Ishman and Sperling, 2002; Mackensen et al., 1990). These upper and lower water column conditions persisted until 6903 yr BP.

Collectively, our data show that the inner Marguerite Bay deglaciation, and the warm early Holocene interval that followed, were associated with modified-UCDW influence throughout the entire water column at our site. This interpretation of modified-UDCW influence on the inner shelf helps explain the rapid retreat of the Marguerite Bay ice stream from at least 9707 yr BP, and subsequent collapse of the George VI Ice Shelf (Bentley et al.,

2011), the rapid thinning of terrestrial ice in inner Marguerite Bay and the onset of marine sedimentation in adjacent fjords (Bentley et al., 2011; Hodgson et al., 2013). Similarly, enhanced upwelling of UCDW onto the shelf prior to ~7 kyr is likely to account for elevated SST (Etourneau et al., 2013; Shevenell et al., 2011) and frontal melting of glaciers (Pike et al., 2013; Fig. 7E) further north at Palmer Deep and the generally warm, limited sea ice conditions experienced throughout the WAP at this time (Bentley et al., 2009; Allen et al., 2010).

4.2 Mid Holocene

From 6903 yr BP the records indicate a decreasing influence of UCDW on inner Marguerite Bay surface waters, marked by extended sea ice seasons and a decline in primary productivity and reduced glacial melt water-derived iron. The presence of ice during the summer months, likely from glacial discharge rather than sea ice, is inferred from increased abundances of *T. antarctica* (cold; Buffen et al., 2007) and low abundances of sea ice species and consistent with the drop in relative SST from 5882 yr BP and reduced flux of planktonic foraminifera to the sea floor. At Palmer Deep, longer sea ice seasons from ~7 kyr BP (Etourneau et al., 2013) and reduced glacial discharge (Pike et al., 2013) also suggest cooling occurred during the mid Holocene at the same time as the ice shelf re-formed in George VI Sound (Fig. 1; Smith et al., 2007; Roberts et al., 2009). The positive shift in our $\delta^{13}C_{N.\ pachyderma\ \text{sin.}}$ record from at least 6992 yr BP is consistent with the decrease in surface water productivity and a reduction in ^{13}C-depleted UCDW mixing through the pycnocline at our site. However, incursions of UCDW into Marguerite Bay continued beneath the pycnocline (Fig. 6C) as indicated by the persistent influx of open ocean *F. kerguelensis* and static benthic $\delta^{13}C$ values. We propose that reduced export of phytodetritus, consistent with the shorter and less productive growth season inferred from the surface ocean records, allowed *B. aculeata* to dominate the benthic foraminiferal assemblage from 6992 to 4153 yr BP.

The mid Holocene cooling trend culminates with lowest relative SSTs in our record and a brief advance of sea ice at 4414 yr BP, preceding a period (4414 to 4153 yr BP) of increased SST and enhanced fluxes of diatoms (Fig. 5B) and planktonic foraminifera. This brief reversal of surface ocean conditions is accompanied by elevated accumulations of a benthic foraminifera assemblage indicative of high phytodetrital fluxes. Warm SSTs, high productivity and the benthic faunal shift indicate that nutrient rich, seasonally stratified surface waters, similar to the early Holocene, were a feature of this interval. However, since planktonic $\delta^{13}C$ does not decrease to early Holocene values, it would appear that mixing of modified-UCDW through the pycnocline did not establish these conditions. Rather, atmospheric warming in the Peninsula region (Mulvaney et al., 2012; Fig. 7D) between 5 and 3 kyr BP is likely to account for enhanced glacial melt along the WAP (Allen et al., 2010; Pike et al., 2013) and may therefore have led to the 260 year re-establishment of early Holocene-like surface conditions within Marguerite Bay from 4414 yr BP. Atmospheric forcing at this time also accounts for ice shelf collapse further north (Pudsey et al., 2006) and generally warm conditions along the Peninsula (Bentley et al. 2009; Allen et al., 2010) centred around ~4 kyr BP (Hodgson et al., 2013).

4.3 Late Holocene

Within Marguerite Bay the transition to a colder late Holocene interval from 4153 yr BP, marked by limited glacier melt water-derived iron, persistently low relative SST and increased sea ice cover is consistent with minimal UCDW influence within surface waters above our site. Both planktonic and benthic foraminifera became scarce, while a relatively high flux of diatoms and Chl*a* from 4414 to 2679 yr BP indicates high export from surface waters. The fluctuating abundance of *T. antarctica* (cold) suggests variable summer sea ice conditions throughout this interval and we therefore propose that the high export resulted

from pulses of intense productivity associated with episodic opening or retreat of sea ice above our site. Episodic overturning of the water column and displacement of UCDW is suggested by the convergence of planktonic and benthic $\delta^{18}O$ records and multi-decadal to centennial scale oscillation between UCDW-indicator *B. aculeata* and agglutinated benthic foraminifera respectively. Unlike calcareous species, agglutinated foraminifera in Antarctic basins have a tolerance to low-temperature and variable-salinity conditions (Ishman & Domack, 1994; Ishman & Sperling 2002).We propose that cool, dense, saline water generated during sea ice formation, periodically sank to the sea floor (Fig. 6D), cooled benthic waters by over 2°C (positive benthic $\delta^{18}O$ excursions of 0.7 ‰) and created unfavourable conditions for calcareous benthic foraminifera species (Ishman & Domack, 1994). Benthic foraminiferal (Ishman & Sperling, 2002) and $\delta^{18}O_{benthic}$ (Shevenell & Kennett 2002) records from ODP 1098, Palmer Deep, suggest that cyclic incursions of UCDW also penetrated the northern WAP shelf from 3.7 kyr BP. The establishment of this episodic overturning of the water column from 4153 yr BP at TPC522 coincides with the interval between 5 and 3.6 kyr BP which appears to mark a period of transition from non-cyclic to cyclic forcing on the WAP recognised in surface ocean records at Palmer Deep (Etourneau et al., 2013; Pike et al., 2013).

From 2679 yr BP the flux of diatoms to our site decreased. The mixed calcareous and agglutinated benthic foraminiferal assemblage throughout the remainder of the record is consistent with continued oscillation between conditions dominated by UCDW upwelling and conditions typical of saline shelf water, although, since the sediment accumulation rate was significantly lower the individual oscillations are not resolved. This drop in sediment accumulation rate may reflect increased frequency of oscillation between these two oceanographic states. More frequent alternation between short-lived intervals of UCDW-upwelling, melting back the sea ice and initiating short-lived intervals of high export flux

associated with and short-lived intervals of shelf water dominated conditions would have allowed benthic organisms to consume and break down phytodetritus, reducing sediment accumulation rates.

4.4 CONTROLS ON UCDW-UPWELLING WITHIN MARGUERITE BAY

Previous studies have failed to achieve a consensus on the influence of UCDW along the WAP through the Holocene (Shevenell & Kennett, 2002; Ishman & Sperling, 2002; see Bentley et al., 2009 for discussion of the conflicting ideas proposed in these papers from Palmer Deep). Pike et al. (2013) also noted inconsistencies between records surface ocean records from Palmer Deep. Our multi-proxy records provide compelling evidence for a decreasing influence of upwelled UCDW within Marguerite Bay through the Holocene. Our interpretation is consistent with a recent proxy record of glacier front melt on the WAP which supports UCDW-driven glacier melt in the early Holocene, shifting towards atmospherically driven-melt in the later Holocene (Pike et al., 2013). The broad correlation of atmospheric temperatures in the Ross Sea region (Steig et al., 1997; Fig. 7C) and SST records within Marguerite Bay suggest a similar climate forcing through the early to mid Holocene. In contrast, atmospheric temperatures recorded in the ice core from James Ross Island in the NW Weddell Sea do not exhibit similar trends, suggesting conditions along the WAP and the Ross Sea shelf were being driven by UCDW-influences rather than atmospheric forcing.

Vigorous upwelling of nutrient-rich CDW during the early Holocene is also evidenced south of the Polar Front by enhanced opal fluxes in the Atlantic and Pacific sectors of the Southern Ocean (Anderson et al., 2009; Fig. 7G). A driver of early Holocene upwelling through the Southern Ocean and WAP could be the strengthening and/or poleward shift in the mean position of the SWW during the last glacial termination (Toggweiler et al., 2006). Although the past position and strength of Last Glacial Maximum SWW remains elusive

(Kohfeld et al., 2013), the mean position of the SWW is proposed to have shifted equatorward during the Holocene (Lamy et al., 2002; Lamy et al., 2010), migrating the core of the Antarctic Circumpolar Current away from the Antarctic continental shelf. More southerly SWW during the early Holocene would therefore have driven more frequent and/or voluminous incursions of warm UCDW onto the continental shelf to mix into surface waters and account for the relatively warm temperatures recorded in the Ross Sea region (Steig et al., 1998) and oceanic archives along the WAP (this study; Allen et al., 2010; Shevenell et al., 2011). Northwards migration of the SWW through the mid Holocene would explain a significant reduction in opal flux south of the Polar Front (Anderson et al., 2009; Fig. 7F), cooling in the Ross Sea region, and is consistent with a decline in UCDW-driven warmth and melt water stratification in Marguerite Bay from 6992 yr BP. By the late Holocene, from 4153 yr BP, only episodic incursions of UCDW entered inner Marguerite Bay and cooler conditions prevailed along the WAP (Allen et al., 2010).

A transition from non-cyclic to cyclic-forcing at Palmer Deep is recognised between 5 and 3.6 kyr BP (Etourneau et al., 2013; Pike et al., 2013; Shevenell & Kennett, 2002). The onset of this cyclic-forcing along the WAP appears to be associated with the waning, non-cyclic influence of the SWW and the increased frequency and/or magnitude of ENSO events from 4.2 kyr BP (Fig. 7A; Conroy et al., 2008; Moy et al., 2002; Pike et al., 2013). From 2.5 kyr BP atmospheric temperatures decrease within the James Ross Island ice core record (Mulvaney et al., 2013) while increasing glacial discharge to ODP Site 1098 (Pike et al., 2013) suggests enhanced atmospheric warming on the WAP. Mulvaney et al (2013) propose that such opposed temperature anomalies on either side of the Peninsula represents the establishment of the Antarctic dipole at 2.5 kyr BP. Proxies of oceanographic conditions however infer that sea surface temperatures remained low and sea ice was prevalent along the WAP throughout the late Holocene (Taylor & Sjunneskog 2002; Bentley et al., 2009; Allen et

al., 2010; this study) indicating that oceanic forcing remained a principle driver of conditions on the WAP shelf. The loss of clearly resolved UCDW-saline shelf water oscillations within our benthic foraminifera assemblage record from 2679 yr BP, considered to reflect increased frequency of water column overturning within Marguerite Bay, is concurrent with a prominent increase in the El Junco sand record indicative of increased ENSO frequency (Conroy et al., 2008). The apparent sensitivity of our record to ENSO frequency during the late Holocene suggests that ENSO exerted an oceanic forcing along the WAP, as well as an atmospheric forcing (Pike at al., 2013) from 4153 yr BP.

5. CONCLUSIONS

Predicted intensification of the SWW through this century (Swart and Fyfe, 2012) demands better understanding of how UCDW upwelling along the WAP responded to changing SWW strength and position through the Holocene. Our multi-proxy record of surface and benthic water conditions provides a comprehensive history of UCDW influence within Marguerite Bay, and demonstrates the apparent responsiveness of UCDW upwelling to SWW through the early and mid Holocene, and to ENSO forcing during the late Holocene.

In recent decades a southward migration and intensification of SWW has been observed (Hande et al., 2012; Swart and Fyfe, 2012). Within the same timeframe increased UCDW upwelling along the WAP has increased heat flux, and likely nutrient flux, onto the continental shelf (Ducklow et al., 2012; Martinson et al., 2008). Basal melting caused by warm modified-UCDW approaching the Getz and Dotson ice shelves (Wåhlin et al, 2010) and Pine Island and Thwaites glaciers on the Amundsen Sea shelf (Jacobs et al., 2011; Walker et al., 2007), and flowing beneath the George VI ice shelf on the Bellingshausen sea shelf (Jenkins and Jacobs, 2008) is the likely cause of accelerated ice sheet thinning in recent years (Pritchard et al., 2012). Similarly, reduced sea ice extent and asymmetrical changes in

Chl *a* along the WAP since the 1980's (Montes-Hugo et al., 2009) suggest a shift towards the early Holocene-like oceanographic configuration reported here. With continued strengthening and poleward migration of the SWW (Swart and Fyfe, 2012), our results show we could anticipate enhanced upwelling south of the Polar Front, and more frequent and persistent incursions of UCDW onto the WAP continental shelf. These are changes that respectively could limit the ability of the Southern Ocean to act as a CO_2 sink (Le Quere et al., 2007), and threaten the stability of the extant ice shelves and feeder glaciers on the WAP.

Acknowledgements

This study is part of the British Antarctic Survey Polar Science for Planet Earth Programme and the Palaeoclimate and Palaeoenvironment core-science programme at the British Geological Survey, funded by the Natural Environment Research Council. We thank the officers and crew of *RRS James Clark Ross* for facilitating recovery of TPC522. Hilary Blagbrough is thanked for providing diatom counts. Stephen Roberts is thanked for generating the age model. We also thank two anonymous reviewers for their constructive comments. James Ralph at the Godwin Lab provided stable isotope analysis. SK publishes with permission of the Executive Director of the British Geological Survey (NERC).

References

Allen, C.S., 2014. Proxy development: A new facet of morphological diversity in the marine diatom Eucampia antarctica (Castracane) Manguin. Journal of Micropalaeontology, doi 10.1144/jmpaleo2013-025

Allen, C.S., Oakes-Fretwell, L.M., Anderson, J.B., Hodgson, D.A. 2010. A record of Holocene glacial and oceanographic variability in Neny Fjord, Antarctic Peninsula. Holocene, 20, 551-564.

Anderson, J.B. 1975. Ecology and distribution of foraminifera in the Weddell Sea of Antarctica. Micropaleontology, 21, 69-96.

Anderson, R. F, Ali, S., Bradtmiller, L. I., Nielsen, S. H. H., Fleisher, M. Q., Anderson, B. E., Burckle, L. H. 2009.Wind-Driven Upwelling in the Southern Ocean and the Deglacial Rise in Atmospheric CO_2. Science 323, 1443-1448.

Appleby, P.G. 2001. Chronostratigraphic techniques in recent sediments. In Last, W.M. and Smol, J.P., editors, Tracking environmental change using lake sediments volume 1: basin analysis, coring, and chronological techniques. Kluwer Academic, 171–203.

Barras, C., Duplessey, J-C, Geslin, E., Michel, E., Jorissen, F. J. 2010. Calibration of $\delta^{18}O$ of cultured benthic foraminiferal calcite as a function of temperature. Biogeosci. 7, 1349–1356.

Bathmann, U.V., Fischer, G., Müller, P.J., Gerdes, D. 1991. Short-term variations in particulate matter sedimentation off Kapp Norvegia, Weddell Sea, Antarctica: relation to water mass advection, ice cover, plankton biomass and feeding activity. Polar Biology 11, 185–195.

Bausch, D., Cartsens, J., Wefer, G. 1997. Oxygen isotope composition of living, Neoglo-boquadrina pachyderma (sin.) in the Arctic Ocean. Earth Planet. Sci. Lett. 146, 47-58.

Bentley M., Hodgson D., Smith J.A., Cofaigh C.O., Domack E., Larter R.D., Roberts S.J., Brachfeld S., Leventer A., Hjort C., Hillenbrand C.D., Evans J. 2009, Mechanisms of Holocene palaeoenvironmental change in the Antarctic Peninsula region. The Holocene, 19, 51–69.

Bentley, M.J., Johnson, J. S., Hodgson, D. A., Dunai, T., Freeman, S. P. H.T., Ó Cofaigh, C. 2011. Rapid deglaciation of Marguerite Bay, western Antarctic Peninsula in the Early Holocene. Quat. Sci. Rev. 30, 3338-3349.

Blaauw, M., 2010. Methods and code for 'classical' age-modelling of radiocarbon sequences. Quaternary Geochronology, 5, 512-518.

Buffen, A., Leventer, A., Rubin, A. Hutchins, T. 2007. Diatom assemblages in surface sediments of the northwestern Weddell Sea, Antarctic Peninsula. Mar. Micropal. 62, 7-30.

Conroy, J. L., Overpeck, J. T., Cole, J. E., Shanahan, T. M., Steinitz-Kannan, M. 2008. Holocene changes in eastern tropical Pacific climate inferred from a Galápagos lake sediment record. Quat. Sci. Rev. 27, 1166-1180.

Ducklow, H. W., Clarke, A., Dickhut, R., Doney, S. C., Geisz, H., Huang, K., Martinson, D. G., Meredith, M. P., Moeller, H. V., Montes-Hugo, M., et al. 2012. The Marine Ecosystem of the West Antarctic Peninsula, in: Antarctica: An Extreme Environment in a Changing World, edited by: Clarke, A., Johnston, N. M., Murphy, E. J.,and Rogers, A. D., Wiley-Blackwell, London, 121–159.

Etourneau, J., Collins, L. G., Willmott, V., Kim, J. H., Barbara, L., Leventer, A., Schouten, S., Sinninghe Damst, S. J., Bianchini, A., Klein, V., Crosta, X., Mass, G. 2013. Holocene climate variations in the western Antarctic Peninsula: evidence for sea ice extent predominantly controlled by insolation and ENSO variability changes. Clim. Past Discuss. 9, 1–41.

Fenner, J., Schrader, H.-J., Wienigk, H. 1976. Diatom phytoplankton studies in the southern Pacific Ocean: composition and correlation to the Antarctic Convergence and its paleoecological significance. *In* Hollister, C.D., Craddock, C., et al., *Init. Repts. DSDP,* 35. Washington (U.S. Govt. Printing Office), 757-813.

Gooday, A.J. 2003. Benthic foraminifera (Protista) as tools in deep-water palaeoceanography: environmental influences on faunal characteristics. In, Southward, A.J., Tyler, P.A., Young, C.M. and Fuiman, L.A. (eds.) Advances in Marine Biology, Vol. 46. London, UK, Academic Press, 3-90.

Gooday, A. J., Hughes, J.A. 2002. Foraminifera associated with phytodetritus deposits at a bathyal site in the northern Rockall Trough (NE Atlantic): seasonal contrasts and a comparison of stained and dead assemblages. Mar. Micropal. 46, 83-110.

Gooday, A. J., Bett, B. J., Jones, D. O. B., Kitazato, H. 2012. The influence of productivity on abyssal foraminiferal biodiversity. Mar. Biodiv. DOI:10.1007/s12526-012-0121-8.

Graham, A.G.C., Smith, J.A., 2012. Palaeoglaciology of the Alexander Island ice cap, western Antarctic Peninsula, reconstructed from marine geophysical and core data. Quat. Sci. Rev. 35, 63-81.

Grossman, E. L. 1987. Stable isotopes in modern benthic foraminifera: a study of vital effect, J. Foramin. Res. 17, 48–61.

Hammer, Ø, Harper, D. Ryan, P. D. 2005. PAST: Palaeontological statistics software package for education and data analysis. Palaeontologia Electronica 4, 9.

Hande, L. B., Siems, S. T., Manton, M. J. 2012. 2012. Observed Trends in Wind Speed over the Southern Ocean. Geophys. Res. Lett. 39, L051734.

Harloff, J., Mackensen, A. 1997. Recent benthic foraminiferal associations and ecology of the Scotia Sea and Argentine Basin. Mar. Micropal. 31, 1-29.

Harris, P. G. Zhao, M., Rosell-Melé, A., Tiedemann, R., Sarnthein, M., Maxwell, J.R. 1996. Chlorin accumulation rate as a proxy for Quaternary marine primary productivity. Nature 383, 63-65.

Hendry, K. R., Rickaby, R. E. M., Meredith, M. P., Elderfield, H. 2009. Controls on table isotope and trace metal uptake in Neogloboquadrina pachyderma (sinistral) from an Antarctic sea-ice environment. Earth Planet. Sci. Lett. 278, 67–77.

Hodgson , D.A., Roberts, S.J., Smith, J.A., Verleyen, E., Sterken, M., Labarque, M., Sabbe, K., Vyverman, W., Allen, C.S., Leng, M.J., Bryant, C., 2013. Late Quaternary environmental changes in Marguerite Bay, Antarctic Peninsula, inferred from lake sediments and raised beaches. Quaternary Science Reviews 68, 216-236.

Igarashi, A., Numanami, H.,Tsuchiya, F., Fukuchi, M. 2001. Bathymetric distribution of fossil foraminifera within marine sediment cores from the eastern part of Lützow − Holm Bay, East Antarctica, and its paleoceanographic implications. Marine Micropaleontology, 42, 125–162.

Ishman, S. E. Domack, E.W. 1994. Oceanographic controls on benthic foraminifera from the Bellingshausen margin of the Antarctic Peninsula. Mar. Micropal. 24, 119-155.

Ishman, S. E., Sperling, M. R. 2002. Benthic foraminiferal record of Holocene deep-water evolution in the Palmer Deep, western Antarctic Peninsula. Geology, 30, 435-438.

Jenkins, A., Jacobs, S. 2008. Circulation and melting beneath George VI Ice Shelf, Antarctica: J. Geophys. Res. 113, JC004449.

Jacobs, S. S., Jenkins, A., Giulivi, C. F., Dutrieux, P. 2011. Stronger ocean circulation and increased melting under Pine Island Glacier ice shelf. Nat. Geosci. 4, 519-523.

Johansen, J. R., Fryxell, G. A. 1985. The genus Thalassiosira (Bacillariophyceae): studies on species occurring south of the Antarctic Convergence Zone. Phycologia 24, 155-179.

Kilfeather, A. A., O Cofaigh, C., Lloyd, J. M., Dowdeswell, J. A. , Xu, S., Moreton, S. G. 2011. Ice-stream retreat and ice-shelf history in Marguerite Trough, Antarctic Penisula: Sedimentological and foraminiferal signatures. Geol. Soc. Am. Bull.123, 997-1015.

Klink, J. M., Hofmann, E. E., Beardsley, R. C., Salihoglu, B., Howard, S. 2004. Water mass properties and circulation on the west Antarctic Peninsula continental shelf in austral fall and winter 2001. Deep-Sea Research II 51, 1925-1946.

Kohfeld, K. E., Graham, R. M., de Boer, A. M., Sime, L.,C., Wolff, E.W., Le Quéré, C., Bopp, L. 2013 Southern Hemisphere westerly wind changes during the Last Glacial Maximum: paleo-data synthesis. *Quat. Sci. Rev.* 68, 76-95.

Kornilova, O., Rosell-Melé, A. 2003. Application of microwave-assisted extraction to the analysis of biomarker climate proxies in marine sediments. Organic Geochem. 34, 1517-1523.

Lamy, F., Ruhlemann, C., Hebbeln, D., Wefer, G. 2002. High- and low-latitude climate control on the position of the southern Peru-Chile Current during the Holocene. Paleoceanography, 17, PA000727.

Lamy, F. Kilian, R., Arz, H. W., Francois, J. P., Kaiser, J., Prange, M., Steinke, T. 2010. Holocene changes in the position and intensity of the southern westerly wind belt. Nat. Geosci. 3, 695-699.

Le Quéré, C. Rodenbeck, C., Buitenhuis, E. T., Conway, T. L., Langenfelds, R., Gomez, A., Labsucchagne, C., Ramonet, M., Nakazawa, T., Metzl, N., Gillett, N. P., Heimann, M. 2007. Saturation of the Southern Ocean CO_2 Sink Due to Recent Climate Change. Science, 316, 1735-1738.

Leventer, A., Domack, E., Barkoukis, A., McAndrews, B., Murray, J. 2002. Lamination from the Palmer Deep: A diatom-based interpretation. Paleoceanography, 17, PA8002.

Mackensen, A. 2012. Strong thermodynamic imprint on recent bottom-water and epibenthic $\delta^{13}C$ in the Weddell Sea revealed: Implications for glacial Southern Ocean ventilation. Earth Planet. Sci. Lett., 317-318, 20-26.

Mackensen, A., Fütterer, D. K., Grobe, H., Schmiedl, G. 1993. Benthic foraminiferal assemblages from the South Atlantic Polar Front region between 35° and 57°S: Distribution, ecology and fossilization potential. Mar. Micropal., 22, 33–69.

Mackensen, A., Grobe, H., Kuhn, G. Fütterer, D. K. 1990. Benthic foraminiferal assemblages from the eastern Weddell Sea between 68 and 73°S: distribution, ecology and fossilization potential. Mar. Micropal. 16, 241-283.

Majewski, W., Anderson, J. B. 2009. Holocene foraminiferal assemblages from Firth of Tay, Antarctic Peninsula: Paleoclimate implications. Mar. Micropal. 73, 135-147.

Martinson, D. G., Stammerjohn, S. E., Iannuzzi, R. A., Smith, R. C., Vernet, M. 2008. Western Antarctic Peninsula physical oceanography and spatio-temporal variability. Deep Sea Res. Pt. II, 55, 1964–1987.

Meredith, M. P., Venables, H. J., Clarke, A., Ducklow, H. W., Erickson, M., Leng, M. J., Lenaerts, J. T. N., Van Den Broeke, M. R. 2013. The FreSWWater System West of the Antarctic Peninsula: Spatial and Temporal Changes. J. Climate. 26, 1669-1984.

Meredith, M. J., Wallace, M. I., Stammerjohn, S. E., Renfrew, I. A., Clarke, A., Venables, H. J., Shoosmith, D. R., Souster, T., Leng, M. J. 2010. Changes in the freSWWater composition of the upper ocean west of the Antarctic Peninsula during the first decade of the 21st century. Prog. Oceanog. 87, 127-143.

Milam, R. W., Anderson, J. B. 1981. Distribution and ecology of recent benthonic foraminifera of the Adelie–George V continental shelf and slope, Antarctica. Mar. Micropal. 6, 297–325.

Moffat, C., Owens, B., Beardsley, R. C. 2009. On the characteristics of Circumpolar Deep Water intrusions to the west Antarctic Peninsula Continental Shelf. J. of Geophys. Res. 114, C05017

Montes-Hugo, M., Doney, S. C., Ducklow, H. W., Fraser, W., Martinson, D., Stammerjohn, S. E., Schofield, O. 2009. Recent Changes in Phytoplankton Communities Associated with Rapid Regional Climate Change Along the Western Antarctic Peninsula. Science, 323, 1470-1473.

Mortyn, P. G. Charles, C. D. 2003. Planktonic foraminiferal depth habitat and ¿^{18}O calibrations: Plankton tow results from the Atlantic sector of the Southern Ocean. Paleoceanography 18, PA000637.

Moy, C. M., Seltzer, G. O., Rodbell, D. T., Anderson D. M. 2002. Variability of El Niño/Southern Oscillation activity at millennial timescales during the Holocene epoch. Nature 420, 162-165.

Mulvaney, R., Abram, N. J., Gagan, M. K., Hindmarsh, R. C. A., Arrowsmith, C., Fleet, L., Triest, J., Sime, L. C., Alemaney, O., Foord, S. 2012. Recent Antarctic Peninsula warming relative to Holocene climate and ice-shelf history. Nature 489, 141-144.

Osterman, L.E., Poore, R.Z., Barron, J. 2001. Climate variability of the Holocene, Site 1098, Palmer Deep, Antarctica. *In* Barker, P.F., Camerlenghi A., Acton, G.D., and Ramsay, A.T.S. (Eds.), *Proc. ODP, Sci. Results*, 178, 1–45.

Pike, J., Crosta, X., Maddison, E. J., Stickley, C. E., Denis, D., Barbara, L., Renssen, H. 2009. Observations on the relationship between the Antarctic coastal diatoms Thalassiosira antarctica Comber and Porosira glacialis (Grunow) Jørgensen and sea ice concentrations during the late Quaternary. Mar. Micropal. 73, 17-25.

Pike, J., Swann, G. E. A., Leng, M. J., Snelling, A. M. 2013. Glacial discharge along the west Antarctic Peninsula during the Holocene. Nat. Geosci. 6, 199-202.

Prézelin, B. B., Hofmann, E. E., Mengelt, C., Klink, J. M. 2000. The linkage between Upper Circumpolar Deep Water (UCDW) and phytoplankton assemblages on the west Antarctic Peninsula continental shelf. J. Mar. Res. 58, 165-202.

Pritchard, H. D. Ligtenberg, S. R. M., Fricker, H. A., Vaughan, D. G., van den Broeke, M. R., Padman, L. 2012. Antarctic ice-sheet loss driven by basal melting of ice shelves. Nature, 484, 502-505.

Pudsey, C. J., Murray, J. W., Appleby, P., Evans, J. 2006. Ice shelf history from petrographic and foraminiferal evidence, northeast Antarctic Peninsula, Quat. Sci. Rev. 25, 2357-2379.

Roberts, S.J., Hodgson, D.A., Bentley, M.J., Smith, J.A., Millar, I., Olive, V., Sugden, D.E., 2008. The Holocene history of George VI Ice Shelf, Antarctic Peninsula from clast-provenance analysis of epishelf lake sediments. Palaeogeography Palaeoclimatology Palaeoecology 259, 258-283.

Rosenheim, B. E., Roe, K. M., Roberts, B. J., Allison, M. A., Kolker, A.S., Johannesson, K. H. 2013. River discharge influences on particulate organic carbon age structure in the Mississippi/Atchafalaya River System. Global Biogeochem. Cycles, 27, 154–166.

Romero, O., Hensen, C., 2002. Oceanographic control of biogenic opal and diatoms in surface sediments of the Southwestern Atlantic. Marine Geology 186 (3–4), 263–280.

Scherer, R. P. 1994. A new method for the determination of absolute abundance of diatoms and other silt-sized sedimentary particles. J. Paleolim. 12, 171-179.

Sen Gupta, B. K., Machain-Castillo, M. L. 1993. Benthic foraminifera in oxygen-poor habitats. Mar. Micropal. 20, 183–201.

Shackleton, N. J. 1974. Attainment of isotopic equilibrium between ocean water and benthonic foraminifera genus Uvigerina: isotopic changes in the ocean during the last glacial. In Labeyrie, L. (ed.): Variation du climat au cours du Pleistocene, 203–209.Colloques Internationau x du Centre Nationale de la Recherche Scientifique 219.

Shevenell, A. E., Ingalls, A. E., Domack, E. W. Kelly, C. 2011. Holocene Southern Ocean surface temperature variability west of the Antarctic Peninsula. Nature, 470, 250-254.

Shevenell, A.E., Kennett, J.P. 2002. Antarctic Holocene climate change: A benthic foraminiferal stable isotope record from Palmer Deep. Paleoceanography, 17, PA000596.

Smith, R. C., Ainley, D., Baker, K., Domack, E., Emslie, S., Fraser, B., Kennett, J., Leventer, A., Mosley-Thompson, E., Stammerjohn, S., M. Vernet. 1999. Marine Ecosystem Sensitivity to Climate Change. BioScience, 49, 393-404.

Smith, J.A., Bentley, M.J., Hodgson, D.A., Roberts, S.J., Leng, M.J., Lloyd, J.M., Barrett, M.J., Bryant, C., Sugden, D.E., 2007. Oceanic and atmospheric forcing of early Holocene ice shelf retreat, George VI Ice Shelf, Antarctica Peninsula. Quaternary Science Reviews 26, 500-516.

Steig, E. J. Brook, E. J., White, J. W. C., Sucher, C. M., Bender, M. L., Lehman, S. J., Morse, D. L., Waddington, E. D., Clow, G. D. 1998. Synchronous climate changes in Antarctica and the North Atlantic. Science, 282, 92-95.

Stickley, C.E., Carter, L., McCave, I.N., Weaver, P.P.E., 2001. Lower circumpolar deep water flow through the SW Pacific Gateway for the last 190 ky: evidence from Antarctic diatoms. In: Seidov, D., Haupt, B., Maslin, M.A. (Eds.), The Oceans and Rapid Climate Change, Past, Present and Future. Geophysical Monograph Series, vol. 126. American Geophysical Union, Washington, D.C., pp. 101–116.

Stickley, C. E., Pike, J., Leventer, A. 2006. Productivity events of the marine diatom Thalassiosira tumida (Janisch) Hasle recorded in deglacial varves from the East Antarctic Margin. Marine Micropaleontology, 59, 184–196.

Stuiver, M., Reimer, P. J. 1993. Extended 14C database and revised CALIB radiocarbon calibration program. Radiocarbon, 35, 215-230.

Swart, N. C., Fyfe, J.C. 2012. Observed and simulated changes in the Southern Hemisphere surface westerly wind-stress. Geophys. Res. Lett. 39, L052810.

Taylor, F., Sjunneskog, C. 2002. Postglacial marine diatom record of the Palmer Deep, Antarctic Peninsula (ODP Leg 178, Site 1089), 2, diatom assemblages. Paleoceanography 17, 8001.

Toggweiler, J. R., Russell, J.L., Carson, S.R. 2006. Midlatitude westerlies, atmospheric CO_2, and climate change during the ice ages. Paleoceanography, 21, PA001154.

Tomas, C. R. 1997. Marine diatoms. In: Tomas, C. R., (Ed.), Identifying marine phytoplankton. Academic press, New York, pp. 5-385.

Vaughan, D.G. Marshall, G. J., Connolley, W. M., Parkinson, C., Mulvaney, R., Hodgson, D. A., King, J. C., Pudsey, C.J., Turner, J. 2003, Recent Rapid Regional warming on the Antarctic Peninsula. Clim. Change, 60, 243-274 (2003).

Wåhlin, A. K., Yuan, X., Björk, G., Nohr, C. 2010. Inflow of Warm Circumpolar Deep Water in the Central Amundsen Shelf. J. Phys. Ocean. 40, 1427-1434.

Walker, D. P. Brandon, M.-A.,Jenkins, A., Allen, J. T., Dowdeswell, J. A.,Evans, J. 2007. Oceanic heat transport onto the Amundsen Sea shelf through a submarine glacial trough. Geophys. Res. Lett. 34, L028154.

Zielinski, U. 1997. Parmales species (siliceous marine nanoplankton) in surface sediments of the Weddell Sea, Southern Ocean indicators for sea ice environment? Mar. Micropal. 32, 387-395.

Figure Captions

Fig. 1. Location of TPC522 (red star) and other sites (numbered in blue) discussed in this paper. 1. Taylor Dome Ice Core (Steig et al., 1997), 2. Chilean Margin (GeoB 3313_1; Lamy et al., 2002), 3. South Atlantic (TN057-13), 4. Tasmanian Gateway (E27-23; Anderson et al., 2009), 5. Adélie Land (MD03-2601; Crosta et al., 2007), 6. Lützow-Holm Bay (Igarashi et al., 2001). On the inset map red arrows indicate the flow of UCDW along the WAP with incursions onto the shelf through bathymetrical lows including Marguerite Trough. Additional sites are; 7. Rothschild Trough (Graham & Smith, 2012), 8. CTD 25; 9-10. Marguerite Bay mid-shelf (Kilfeather et al., 2011); 11. Ryder Bay, Rothera Oceanographic and Biological Time-Series site (Hendry et al., 2009), 12. Neny Fjord, (Allen et al., 2010), 13. Palmer Deep (Taylor & Sjunneskog, 2002; Ishman & Sperling, 2002; Shevenell & Kennett, 2002, Shevenell et al., 2011; Etourneau et al., 2013); 14. Maxwell Bay (Milliken et al., 2009), 15. Firth of Tay (Michalchuk et al., 2009; Mayewski & Anderson, 2009), 16. James Ross Island Ice Core (Mulvaney et al., 2012).

Fig. 2. Modern temperature and salinity profile and predicted $\delta^{18}O_{CaCO3}$ within Marguerite Trough. (A) temperature (red) and salinity (green) from CTD25 (Number 8; Figure 1)

collected 2nd April 2008. Antarctic Surface Water (AASW), Winter Water (WW), modified-UCDW (m-UCDW), (B). predicted $\delta^{18}O_{CaCO3}$ calculated from temperature and salinity following Shackleton (1974). Mean $\delta^{18}O$ *N. pachyderma* sin. (after vital effect correction of 0.63 ‰ from BC523 surface sediments is shown by a red data point with horizontal bars showing standard deviation and vertical bars showing the corresponding calcification depth based on modern predicted $\delta^{18}O_{CaCO3}$. Average $\delta^{18}O$ *B. aculeata* from BC523 surface sediments is shown by the blue data point with horizontal bars showing standard deviation confirming that *B. aculeata* calcifies close to equilibrium with seawater $\delta^{18}O$. Note that TPC522 is at 910 m water depth.

Fig. 3. A. Age-depth model of TPC522. Calibrated AIOM radiocarbon dates shown in blue. Green data point is the calibrated radiocarbon date derived from *Globocassidulina biora* and the red data point is the omitted AIOM date. Black line is the best fit with the grey lines indicating the 95% confidence interval. Sedimentation rates (cm yr^{-1}). B. Excess ^{210}Pb activity in the upper 24 cm of BC523 demonstrating recent deposition of the surface sediment.

Fig. 4. Correspondence analysis of (A) diatom and (B) benthic foraminifera assemblages from PC522 showing the first three axes. Open symbols in B indicate samples where less than 50 individual benthic foraminifera specimens were counted. Vertical white shading bordered by grey lines indicates the standard deviation (1 s.d.) of the data on each axis. Points beyond 1 s.d. are significant and were used to determine stratigraphic boundaries between assemblages. Three principal assemblages were identified in each record corresponding to the early Holocene (yellow), mid Holocene (green) and late Holocene (blue). The darker blue

interval within the late Holocene assemblage indicates an interval of high sedimentation rates and improved temporal resolution where oscillatory trends can be identified.

Fig. 5. Multi-proxy Holocene surface and benthic records from Marguerite Bay, TPC522. The upper panel shows the surface ocean records and the bottom panel shows benthic foraminifera assemblages, and benthic and planktonic stable isotope records. Upper panel, (A) ice rafted debris concentration (# grains >150μm g^{-1}; dark blue) and magnetic susceptibility (grey), (B) total diatom flux (# cm^{-2} kyr^{-1}), (C) Chl *a* concentration (abs at 410 nm g^{-1}), (D) *Fragilariopsis curta*: *Fragilariopsis kerguelensis* ratio (E) *Thalassiosira antarctica* (cold) %, (F) *Eucampia antarctica* %, (G) relative SST proxy *E. antarctica* asymm:symm, open symbols indicate samples were less than 100 specimens were counted, (H) flux of planktonic foraminifera *N. pachyderma* sin. (# cm^{-2} kyr^{-1}). Coloured horizontal bars indicate distinct stratigraphic intervals in the diatom assemblages as shown in Fig. 4A. which correspond to the early Holocene, 9707 to 6903 yr BP (yellow); mid Holocene, 6903 to 4213 yr BP (green); late Holocene, 4213 to 825 yr BP (blue). Lower panel, (I) Benthic foraminifera accumulation rate (# cm^{-2} kyr^{-1}), (J) Benthic foraminifera species diversity (Fischer Alpha), (K) *Fursenkoina fusiformis* %, (L) *Nonionella* spp. %, (M) agglutinated species %, (N) *Bulimina aculeata* %, Open symbols indicate samples where less than 50 individual benthic foraminifera specimens were counted, paler coloured infill indicate samples where between 50 and 100 specimens were counted, fully filled symbols indicate that >100 specimens were counted. (O) benthic (*B. aculeata*; blue) and planktonic (*N. pachyderma* sin.; red) $\delta^{13}C$. Dashed line at 0.4 ‰. $\delta^{13}C$ <0.4 ‰ indicates a diagnostic UCDW signal within the water mass (Mackensen, 2012), (P) benthic (*B. aculeata*; blue) and planktonic (*N. pachyderma* sin.; red) $\delta^{18}O$. Open symbols indicate samples where less than 10 specimens were analysed. Coloured horizontal bars indicate stratigraphic intervals distinct

benthic foraminifera assemblages as Fig. 4B. which correspond to the early Holocene, 9707 to 6992 yr BP (yellow); mid Holocene, 6992 to 4153 yr BP (green); late Holocene, 4153 to 825 yr BP (blue). In both panels the early Holocene, prior to 9707 kyr BP, is shown in grey. The darker blue interval within the late Holocene assemblage indicates an interval of high sedimentation rates and improved temporal resolution where oscillatory trends can be identified until 2679 yr BP. The grey dashed lines indicate the interval of early Holocene-like conditions at the transition from mid to Late Holocene.

Fig. 6. Schematic diagram of factors affecting surface and benthic proxy records at TPC522, Marguerite Bay through the Holocene. (A) Early Holocene. Initial incursion of UCDW associated with retreat of the Marguerite Bay ice stream past TPC522, (B) Early Holocene. Persistent incursions of UCDW penetrate inner Marguerite Bay and mix through the pycnocline, limiting sea ice and promoting glacial melt and primary productivity. High phytodetritus fluxes to sea floor, (C) Mid Holocene. UCDW continues to penetrate inner Marguerite Bay but does not mix through the pycnocline as vigorously as in the early Holocene. Lengthening sea ice season and decreased glacial melt causes productivity to fall resulting in a reduced flux of phytodetritus to the sea floor, (D) Late Holocene. Episodic oscillation between UCDW incursions opening up sea ice and promoting pulses of productivity and, generation of cold, dense brines as sea ice reforms which displace UDCW as they sink to the seafloor. Relative size of red arrows represents the relative intensity of UCDW incursions and mixing. Blue arrows indicate cold, dense saline waters produced during sea ice formation. Site TPC522 indicted with yellow circle in (A). (E) Marguerite Bay today (after Moffat et al., 2009). UCDW incursions into Marguerite Bay are associated with reduced sea ice and enhanced glacier melt relative to the late Holocene. Given that there is no evidence for major glacier readvance within Neny Fjord through the Holocene (Allen et al.,

2010) the glacial margin around Marguerite Bay is illustrated as being fixed through the last 9707 yr within these schematics.

Fig. 7. Holocene record of UCDW upwelling at Marguerite Bay compared with (A) Relative frequency of ENSO events inferred from sand % within El Junco crater lake sediments, Galapagos Islands (Conroy et al., 2008). (B), relative SST within Marguerite Bay inferred from the ratio of asymmetrical:symmetrical forms of *E. Antarctica*, (C) Taylor Dome δD that documents the relative atmospheric temperature in the Ross Sea Embayment (Steig et al., 1998; 5 point-running average), (D) James Ross Island ice core temperature anomaly that records temperatures in the NW Weddell Sea (Mulvaney et al., 2012), (E) Diatom $\delta^{18}O$ from ODP Site 1098 (Pike et al., 2013), (F) relative glacial meltwater flux within Marguerite Bay inferred from the relative abundance of *E. antarctica* in TPC522, (G) opal fluxes south of the Polar Front at TN057-13, SE Atlantic and E27-23, SW Pacific (Anderson et al., 2009). Coloured horizontal bars as Fig. 5 (lower panel) with the addition of an outlined green bar indicating the transition of non-cyclic to cyclic forcing observed at Palmer Deep (Pike et al., 2013). Panel to the right summarises our interpretation of UCDW influence in inner Marguerite Bay.

Lab code	Site	Core depth (cm)	Material dated	Conventional radiocarbon age (yrs BP ± 1σ)	Calibrated age range 95% confidence (cal yrs BP)	Total Organic carbon (%)	$\delta^{13}C_{TOC}$ (‰)
SUERC-23333	BC521	SURFACE	Organic carbon	1728 ±37		1.3	-23.0
SUERC-23334	BC523	SURFACE	Organic carbon	1778 ±37		1.2	-23.1
BETA-285245	TPC522	0	Organic carbon	2090 ±40	292 - 461	1.3	-22.7
BETA-271279	TPC522	2	Organic carbon	3070 ±40	1179 - 1345	1.4	-21.4
BETA-285244	TPC522	66	Organic carbon	4080 ±40	2324 - 2601	1.6	-21.4
SUERC-23814	TPC522	150	Organic carbon	4669 ±40	3043 - 3305	1.7	-22.0
BETA-271280	TPC522	250	Organic carbon	5350 ±40	3882 - 4131	1.6	-21.4
BETA-282631	TPC522	350	Organic carbon	6420 ±40*		1.6	-21.0
BETA-271281	TPC522	450	Organic carbon	5870 ±40	4508 - 4821	1.5	-21.0
BETA-282632	TPC522	550	Organic carbon	6930 ±40	5882 - 6094	1.4	-21.8
BETA-271282	TPC522	650	Organic carbon	8140 ±40	7239 - 7405	1.5	-20.5
BETA-282633	TPC522	750	Organic carbon	8760 ±40	7779 - 7955	1.4	-20.8
BETA-271283	TPC522	850	Organic carbon	9390 ±40	8399 - 8582	1.5	-21.5
BETA-282634	TPC522	955	Organic carbon	10360 ±50	9536 - 9863	0.9	-21.4
BETA-282635	TPC522	1000	*G. biora*	10250 ±40	9470 - 9661	-	-

1

Table 1. Radiocarbon dates from TPC522 and box core surface samples from BC521 and BC523.

Figure 1

Click here to download high resolution image

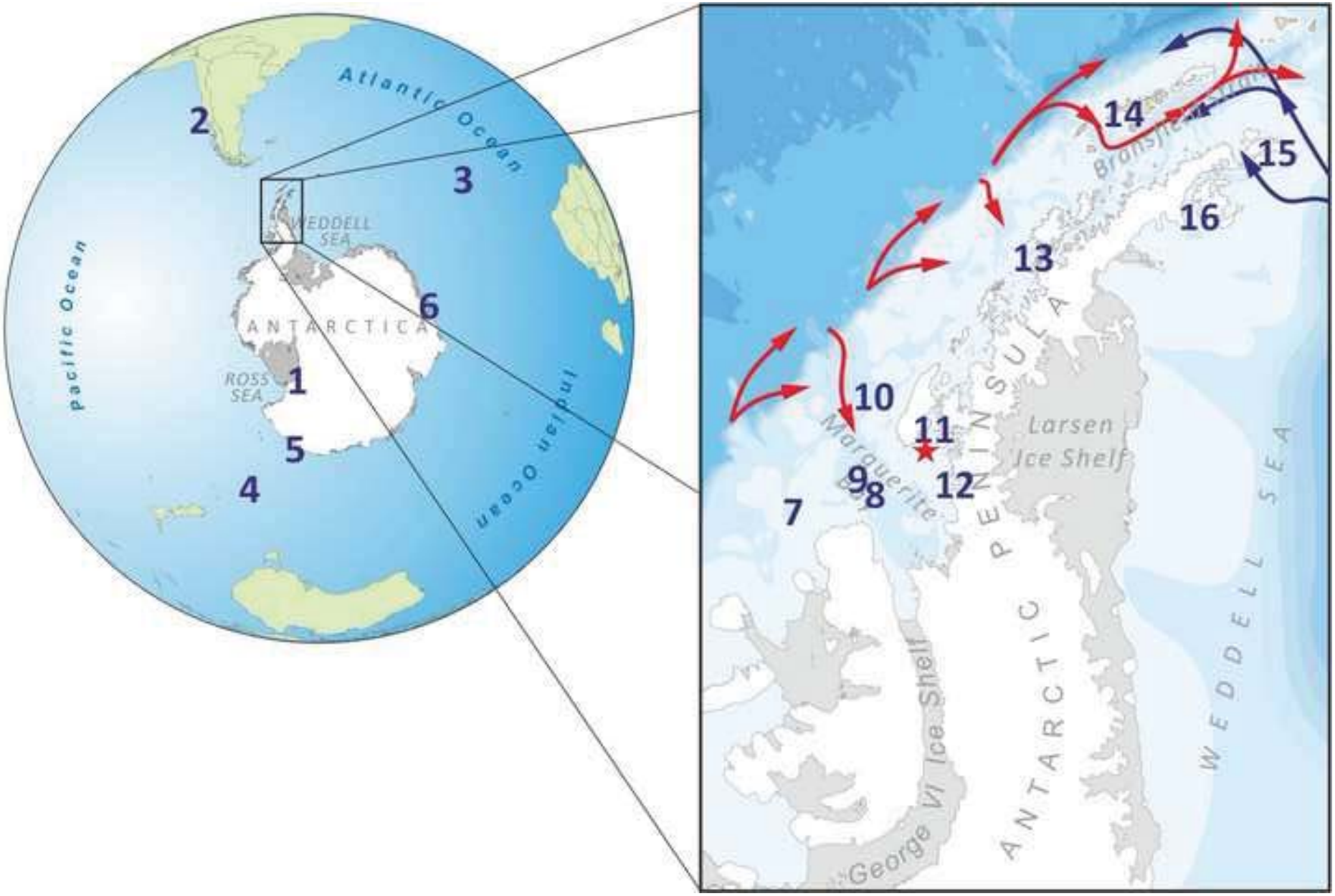

Figure 2
Click here to download high resolution image

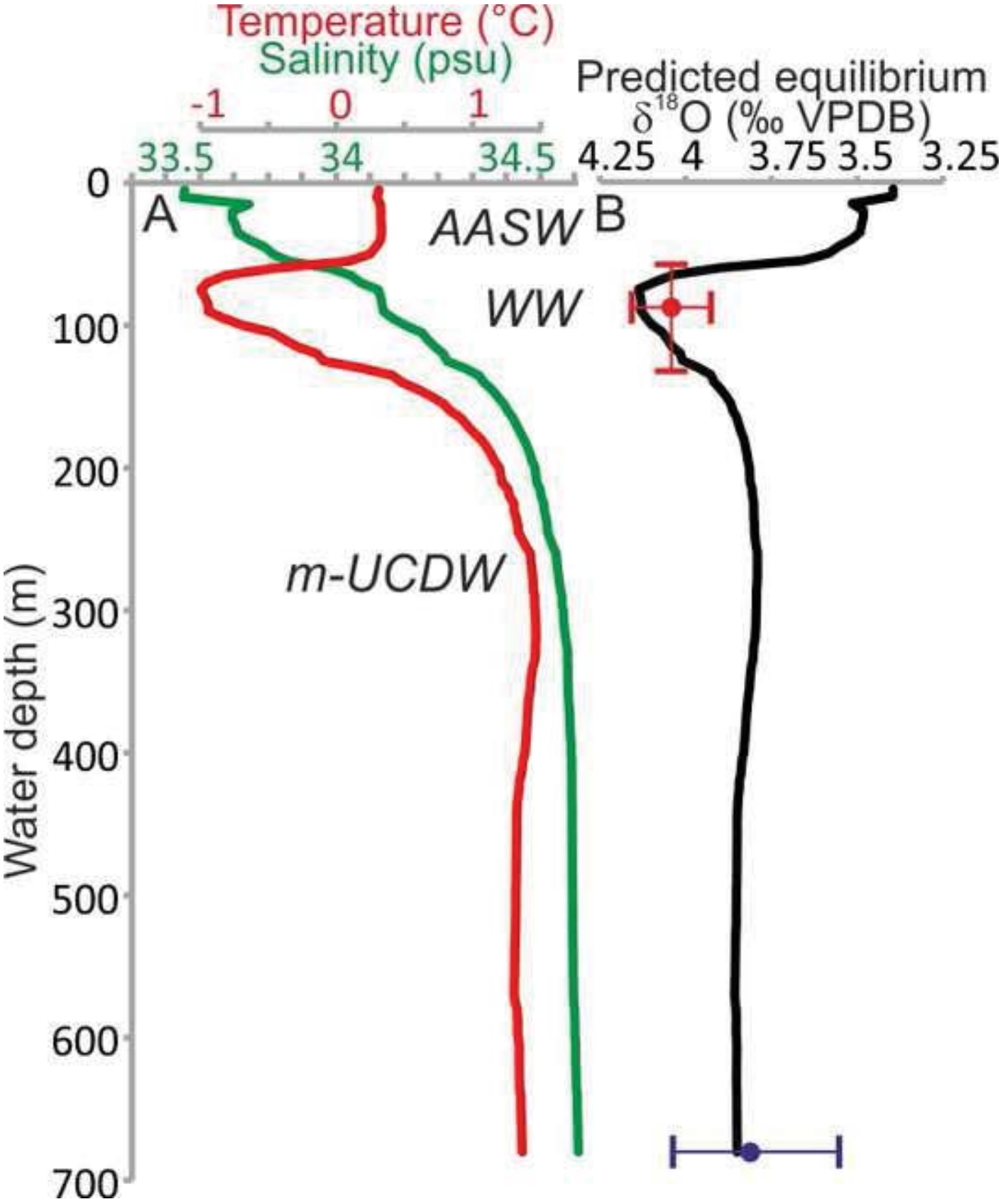

Figure 3

Click here to download high resolution image

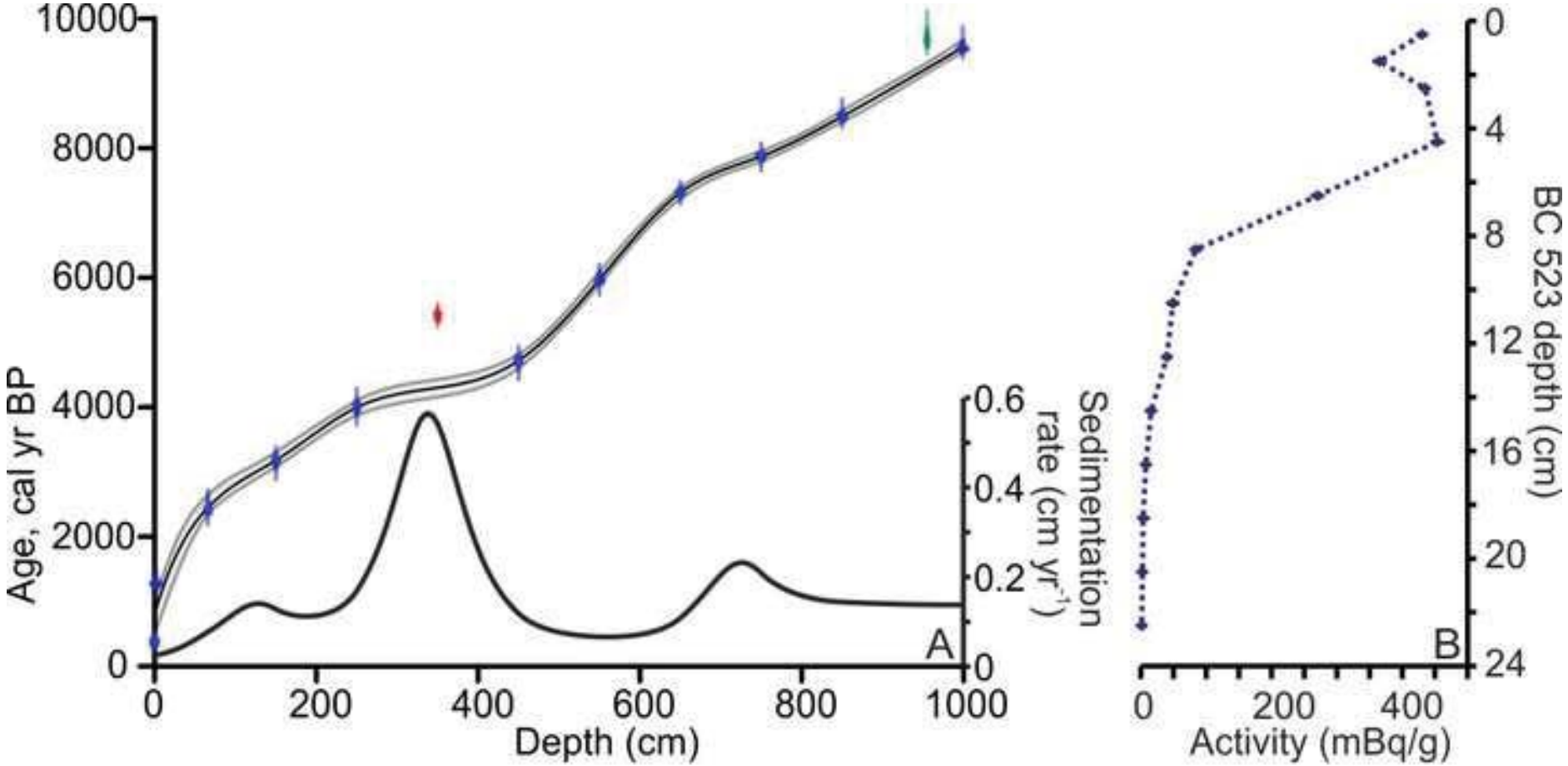

Figure 4

Click here to download high resolution image

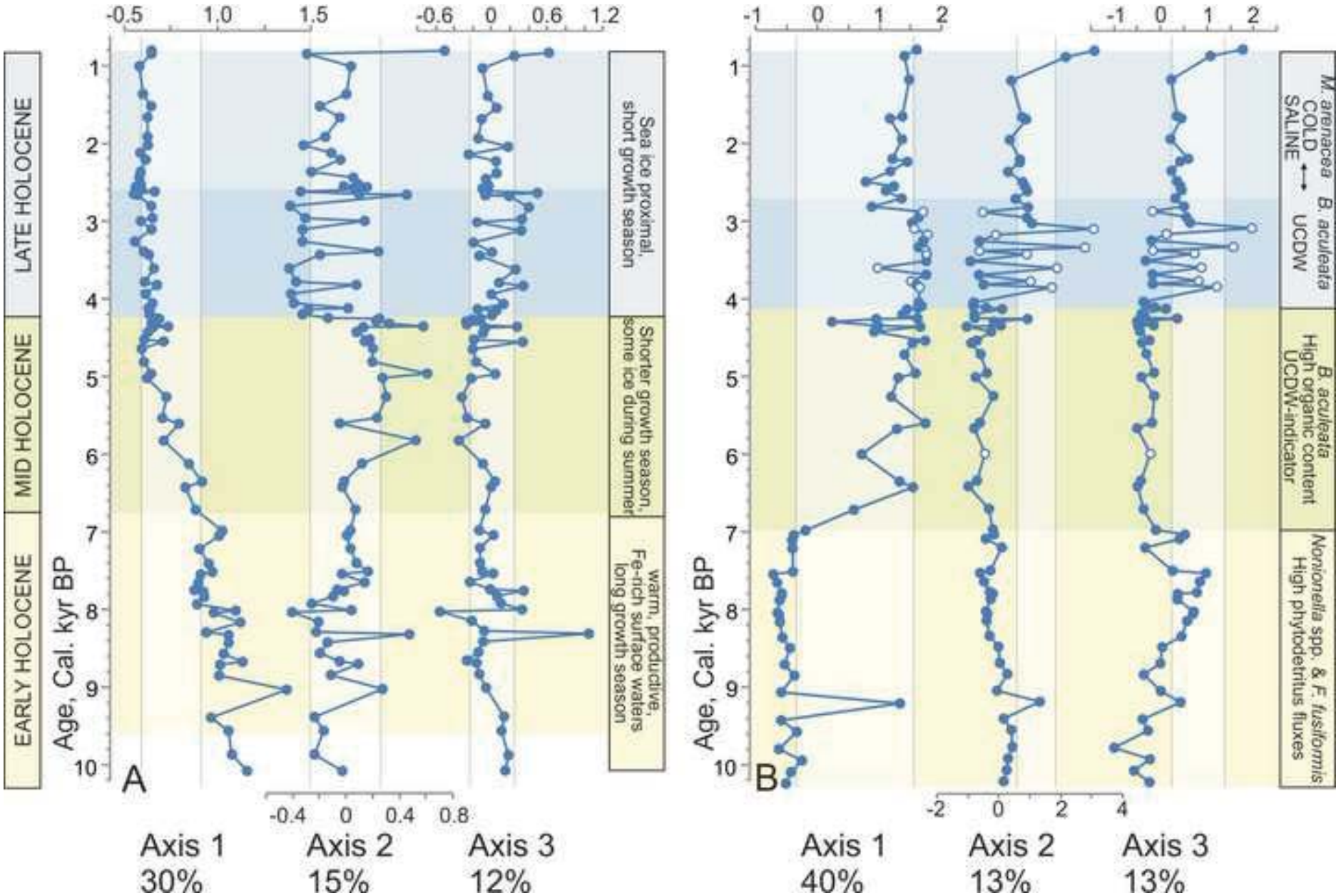

Figure 5
Click here to download high resolution image

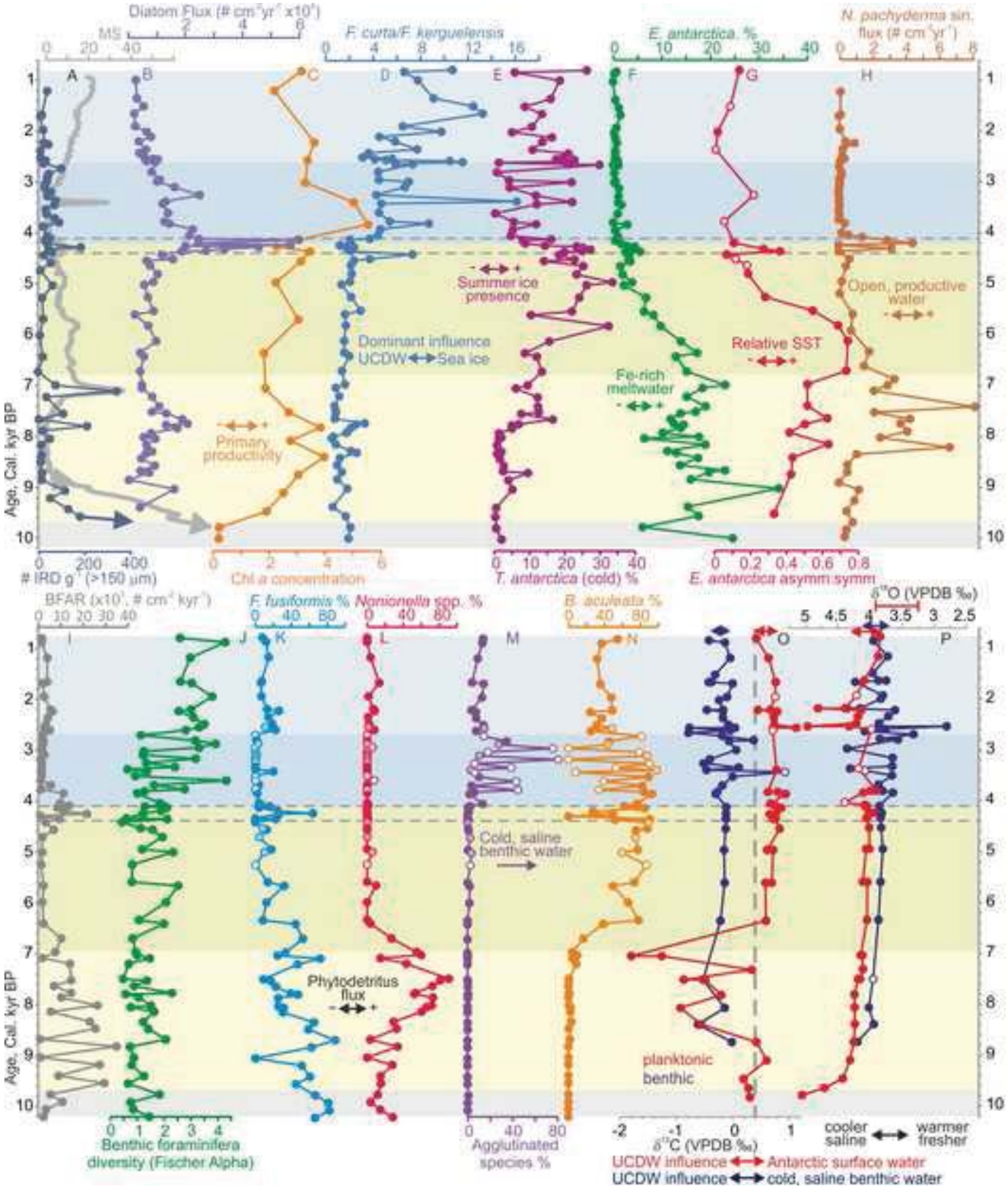

Figure 6

Click here to download high resolution image

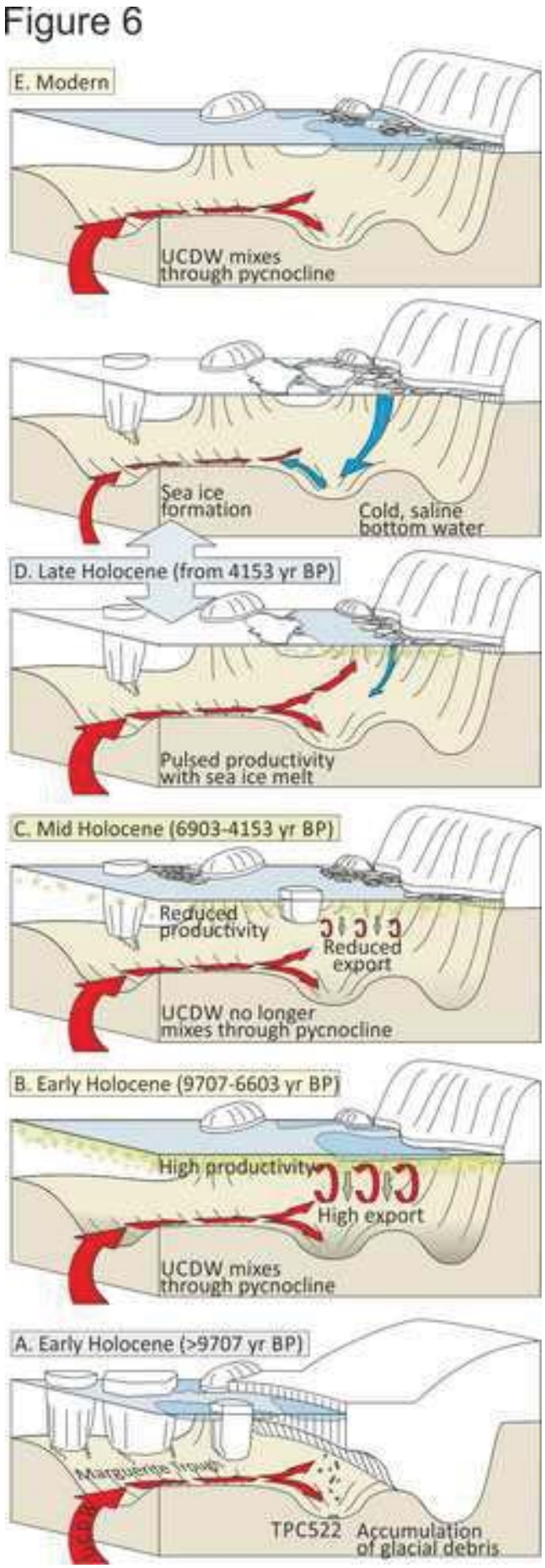

Figure 7

Click here to download high resolution image

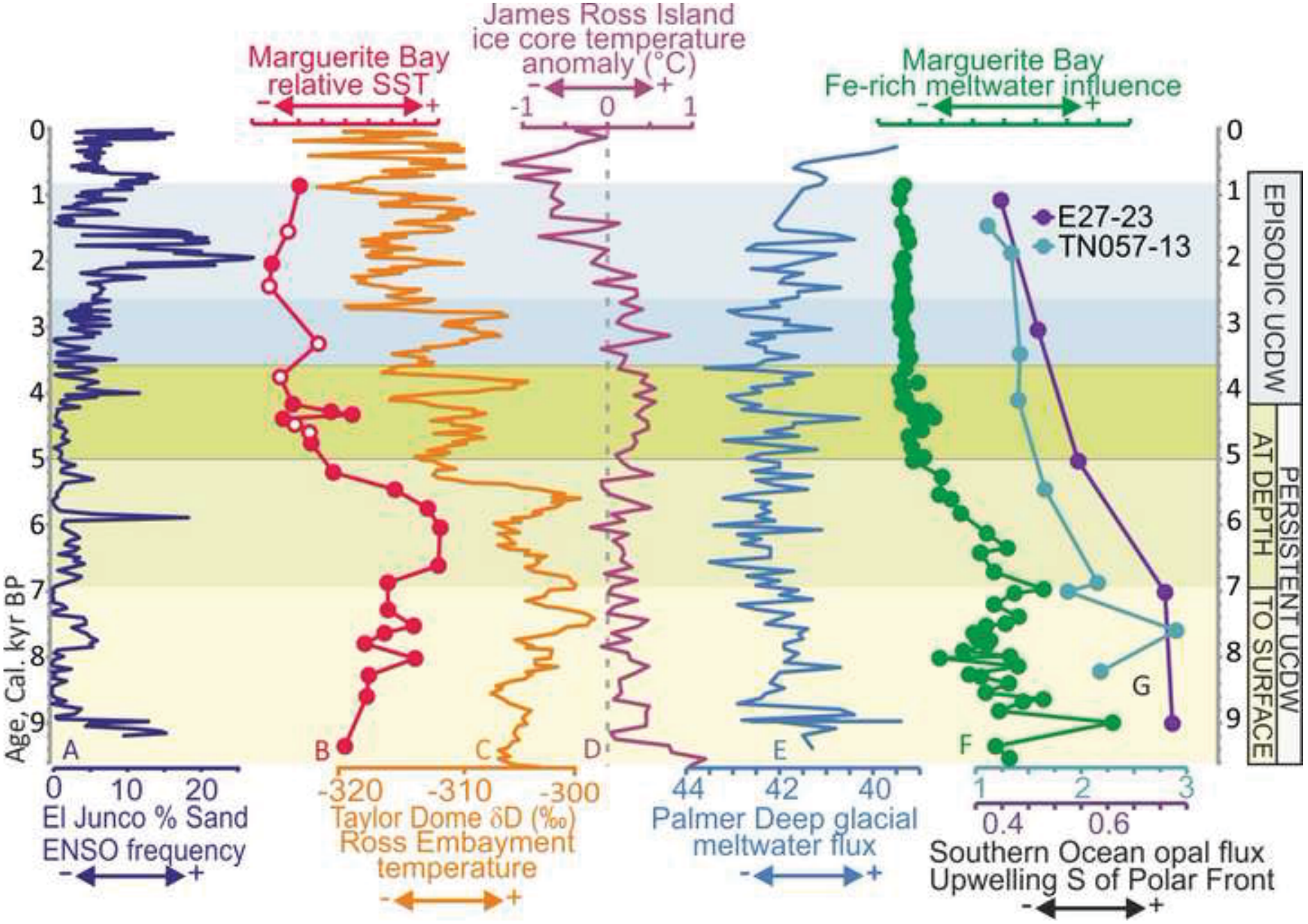

Supplementary Data

Click here to download Supplementary Data: Supplementary material.doc